frontiers | Frontiers in Materials

TYPE Original Research
PUBLISHED 13 November 2024
DOI 10.3389/fmats.2024.1443216

OPEN ACCESS

EDITED BY
Mijia Yang,
North Dakota State University, United States

REVIEWED BY
Peng Zhang,
Zhengzhou University, China
Asif Jalal,
North Dakota State University, United States

*CORRESPONDENCE
Urs Buegger,
urs.buegger@tu-braunschweig.de

RECEIVED 03 June 2024
ACCEPTED 21 October 2024
PUBLISHED 13 November 2024

CITATION
Buegger U, Carvalho EB, Jänicke R and Tofeti Lima T (2024) Assessment of the self-healing capacity of PVA fiber-reinforced composites by chloride permeability and stiffness recovery.
Front. Mater. 11:1443216.
doi: 10.3389/fmats.2024.1443216

Assessment of the self-healing capacity of PVA fiber-reinforced composites by chloride permeability and stiffness recovery

Urs Buegger[1]*, Eliane Betania Carvalho[2], Ralf Jänicke[1] and Thamara Tofeti Lima[1]

[1]Institute of Applied Mechanics, Technical University Braunschweig, Braunschweig, Germany, [2]Department of Civil Engineering, Federal University of Uberlandia, Uberlandia, Brazil

This paper investigates the intrinsic ability of PVA fiber-reinforced cementitious composites to re-establish the durability properties of the uncracked state. Comparative chloride penetration tests are used as a direct measure to quantify the effect of self-healing on the chloride penetration resistance after cracking. Two different composites with cement to fly ash ratios of 1:1.5 and 1:2.0 were studied under the influence of healing periods of up to 28 days. After inducing cracks between 100 and 120 µm, samples were exposed to chlorides for 72 h and the resulting chloride penetration depth was compared to the unhealed state. Based on this procedure, a durability recovery index was proposed to quantify the material's ability to re-establish its function as a protective layer after cracking. Results show that after 14 days of self-healing, chloride penetration through cracks was reduced between 81% and 99%. An extended healing period of 28 days leads to further reduction of the penetration depth to 84%–100%, indicating that most of the reaction takes place within the first 14 days of healing. While the stiffness recovery analysis showed that increasing cement content by 20% correlated with the formation of stronger healing products, no significant difference was found regarding crack closure.

KEYWORDS

durability, self-healing, crack sealing, chloride penetration, PVA fibers, stiffness recovery

1 Introduction

Concrete structures may degrade over time due to prolonged exposure to environmental factors, gradually compromising their performance and structural integrity. Deterioration processes that include chloride-induced corrosion, freeze-thaw cycles, and exposure to aggressive environments have been widely recorded, often resulting in brittle failures as a drastic outcome (Bijen, 2003; Krentowski, 2021; Alexander and Beushausen, 2019). It is known that the presence of cracks significantly impacts the durability of concrete. While cracks themselves may not always lead to immediate damage, they do provide pathways for aggressive ions to penetrate the structure over time (Shobana et al., 2021; Jiangtao et al., 2021). Recognizing the importance of durability in design is crucial, despite the considerable challenges in accurately predicting it (Polder et al., 2012; Neville, 2001; Mehta, 1991). To fully

integrate durability into a structure's service life, a shift towards a performance-based design approach using highly durable materials that can be tailored to achieve specific material properties is necessary.

Fiber-reinforced composites, such as Engineered Cementitious Composites (ECCs), have been developed to address the brittleness of cementitious materials. The primary aim is to bridge cracks that form in the matrix when the material is stressed, which provides post-cracking ductility, thereby enhancing resilience and improving long-term durability (Li, 2019; Casini, 2022). ECCs are characterized by a tensile strain capacity typically beyond 3% and a controlled crack opening (Li, 1998; Li et al., 2001; Li, 1992). Compared to normal concrete, ECCs feature much narrower crack widths, usually around 60 μm (Li, 2019), even at extremely high strains.

The standard ECC mix design called M45 was developed by Victor Li (Li, 1993) and is comprised of ordinary portland cement (OPC), fly ash, silica sand, and polyvinyl alcohol (PVA) fibers at 2% in volume (Li, 2019). The high binder content of this mix design coupled with a low water/binder (w/b)-ratio that typically does not exceed 0.30 (Zhu et al., 2022; Cai et al., 2023) results in its proven ability to self-heal. The lack of water means that many binder particles do not react during the initial hydration reaction. After cracking occurs and penetrating water reaches these unhydrated particles, the subsequent hydration reaction can effectively close cracks provided they do not exceed a certain crack width.

Self-healing materials can significantly address the issues associated with concrete cracking, thereby lowering maintenance costs over a structure's service life and increasing its lifespan (Chen et al., 2022). The motivation to center this study around durability lies in the material's intrinsic capability to re-establish the durability properties of the uncracked state after cracking. When cracks form in structures, the layer of concrete protecting the embedded rebar from aggressive ions, such as chlorides, is locally destroyed. Through self-healing these cracks can be sealed and the protection can be re-established.

This behavior calls for an evaluation of self-healing by quantifying the effects on the durability properties, specifically the penetration resistance to chlorides, rather than just measuring crack closure over time. Since there are still no established analysis methods, the authors propose to use chloride permeability to quantify the "durability recovery" of the material. Crack closure facilitated by self-healing (Ruan et al., 2021; Öztürk et al., 2020) as well as permeability (Zeng et al., 2020; Plagué et al., 2017; Lepech and Li, 2009) have been studied thoroughly for both conventional concrete and fiber-reinforced composites. However, there are few studies directly tying self-healing to the penetration depth of chlorides through an individual crack. The extent of this proposed durability recovery is measured through comparative chloride penetration tests of cracked specimens and specimens that have healed for different periods of time and is expressed through a durability recovery index. The benefit of this approach is obtaining a measure that directly reflects the impact of self-healing on the durability of a structure under realistic conditions.

As a first step, the behavior of the composite is investigated and defined in terms of the fiber distribution, its strain hardening capacity, and crack pattern formation. In order to quantify the strain capacity and describe the cracking behavior of the material, the specimens are subjected to a four-point bending test (4PBT). This will give a general overview of the mechanical properties of the composite. Subsequently, self-healing is assessed through two measurements: (i) chloride penetration to visualize and quantify water permeability before and after healing, and (ii) stiffness recovery associated with the healed cracks. Quantifying stiffness recovery on top of self-healing aims to provide insight into the strength of these newly formed reaction products and how they are influenced by the composition of the composite. For these experiments, a three-point bending test (3PBT) setup is chosen over a four-point bending test (4PBT) as it enables a more accurate evaluation of a specific crack width. This study considers two different mixes varying the ratio of OPC to fly ash is varied between 1:1.5 and 1:2, while keeping the total amount of binder constant.

2 Materials and methods

2.1 Materials and mix design

Two different mix designs were used in this study (Table 1). In mix M1.5 the binder comprises one-part OPC (CEM I 52.5 R according to the EN 197–1 standard) and 1.5 parts fly ash (PFA), while in mix M2.0 it consists of one-part OPC and two parts PFA. The total amount of binder and the water/binder-ratio were kept constant. Table 2 shows the chemical composition of the raw binders and fineness of OPC. The volume of PVA fibers of type RF400, produced by Kuralon Japan, was kept constant at 2% for both mixes. Properties of the PVA fibers according to the manufacturer can be found in Table 3. The addition of high quantities of fibers typically leads to issues with workability that need to be countered with the use of chemical admixtures. Sika Viscocrete 1,079 was used as a superplasticizer. The dosage can be found in Table 1 and was tailored so that both mix designs reached a comparable spread diameter in flow table tests.

2.2 Mixing, casting, and curing

To ensure a uniform distribution of the mix components, the binder paste was mixed before adding the sand and fibers. Moreover, a better coating with the paste can be achieved by slowly adding the sand and fibers into the binder paste (França, 2018). Cement and fly ash were first dry-mixed for about 10 s. Then, water and superplasticizer were added and mixed for 60 s leading to a very liquid binder paste. During continued mixing of the paste, first the silica sand was slowly added to the mix over the course of about 20 s. After, the fibers were dispersed by hand and added into the revolving mix over the course of 60 s. Once all components had been added, the mixture was mixed for another 60 s and then poured into the formwork. Immediately after casting, the specimens were covered with plastic foil to prevent excess evaporation. Specimens were demolded 48 h after casting and cured in a water tank for 28 days.

2.3 Specimens

A total of 24 beams were cast for this study. The dimensions of the beams were 25 cm in length, 4 cm in width, and 4 cm in height.

TABLE 1 Quantities of materials in kg per m^3 of both mix designs.

Mix	CEM I 52.5 R	Fly ash	Silica sand 0/2	Water (water/binder)	Superplasticizer (M-% of binder)	PVA fibers (Volume-%)
M1.5	468	702	440	351 (0.3)	6 (0.5)	26 (2.0)
M2.0	386	772	440	347 (0.3)	4.8 (0.4)	26 (2.0)

TABLE 2 Chemical composition of binder materials and fineness of OPC obtained by the manufacturer.

Chemical composition (%)								
Binder	CaO	SiO_2	Al_2O_3	Fe_2O_3	MgO	SO_3	Ignition Loss (%)	Fineness (cm^2/g)
OPC	63.2	20.0	4.1	1.9	4.2	3.4	0.8	3,120
PFA	3.3	54.2	20.5	6.3	1.5	0.06	4.18	-

TABLE 3 Mechanical and geometrical properties of the PVA fibers.

Type	Diameter (μm)	Length (mm)	Density (g/cm^3)	Tensile strength (MPa)	Elongation (%)	Young's modulus (MPa)	Aspect ratio (L/d)
RF400	200	12	1.3	975	9	27	60

While the length of the beam is determined by the limitations of the test equipment, the cross section of 4 cm × 4 cm is determined by the necessity to cut samples of the beam in order to analyze the chloride penetration as described in Section 2.5.3. Table 4 gives an overview of the naming regime, curing ages of the beams, and purpose of the respective tests.

2.4 Mechanical properties

The mechanical performance of fiber-reinforced composites is greatly influenced by the fiber orientation and distribution (Sarmiento et al., 2016; Tawfek et al., 2023). A uniform distribution of fibers within the composite is an essential factor for the development of both a pronounced strain hardening behavior and a distributed cracking pattern (Kang and Kim, 2011). However, improper dosage of admixtures can lead to detrimental effects such as segregation or bleeding (Passuello et al., 2009; Felekoglu et al., 2014). To verify that a random distribution of the fibers was achieved, the specimens were scanned by X-ray computed tomography (XRCT). To that end, cores with a diameter of 20 mm were drilled from beams of both mix designs, dried in the oven at 60°C for 24 h and then scanned. Due to the large difference in X-ray absorption between the cementitious matrix and the fibers, the fibers can be isolated using a greyscale segmentation and visualized separately as shown in Figure 1.

Generally, the fibers are well distributed throughout the matrix without visible agglomerations. In the top left corner of Figure 1B, however, a slight alignment of the fibers can be observed, where some of the fibers appear to be inclined at an angle of around 10°–20° relative to the plane of the cylinder. The alignment can be attributed to the flow direction during the casting process, but it is not expected to have a significant impact on the mechanical properties.

Four-point bending tests were conducted using a universal testing machine (Zeiss Z050) in order to quantify the mechanical properties of the material. The loading span and support span were 70 mm and 230 mm, respectively. The test was under displacement control with a loading speed of 0.1 mm/min until a displacement of 0.1 mm and then increased to 0.3 mm/min. A linear variable differential transformer (LVDT) was installed at the bottom of the samples to measure the tensile deformation of the gauging zone of 100 mm. M1.5-ULT56-1 and M1.5-ULT56-2 exhibited peak stresses of 4.7 MPa and 4.5 MPa at 0.6%–1.0% strain, respectively, while M2.0-ULT56–1 and M2.0-ULT56-2 showed peak stresses of 3.7 MPa and 6.7 MPa at 1%–2% strain. Digital image correlation (DIC) was applied to visualize the strain field and analyze the cracking behavior of the specimens. Cracks were captured using the high-resolution camera "U3-3990SE-M-GL Rev.1.2" manufactured by IDS Imaging. DIC analysis was performed using the software GOM Correlate, integrated into the ZEISS Quality Suite. Figure 2 illustrates the formation of multiple cracks in the midsection of the beams in the 4PBT setup.

2.5 Test procedures

2.5.1 Pre-cracking (3PBT)

For the pre-cracking process, a target crack opening width of 100–120 μm was selected. Studies confirm that cracks below

TABLE 4 Overview of the specimens.

Mix	Name	# of specimens	Curing age [d]	Healing period [d]	Test goal
M1.5	ULT56	2	56	-	Strain capacity at 56 days
	CRK	2	28	-	Chloride penetration without healing
	RECRK14	2	28	14	Stiffness recovery after 14 days of healing
	HEAL14	2	28	14	Chloride penetration after 14 days of healing
	RECRK28	2	28	28	Stiffness recovery after 28 days of healing
	HEAL28	2	28	28	Chloride penetration after 28 days of healing
M2.0	ULT56	2	56	-	Strain capacity at 56 days
	CRK	2	28	-	Chloride penetration without healing
	RECRK14	2	28	14	Stiffness recovery after 14 days of healing
	HEAL14	2	28	14	Chloride penetration after 14 days of healing
	RECRK28	2	28	28	Stiffness recovery after 28 days of healing
	HEAL28	2	28	28	Chloride penetration after 28 days of healing

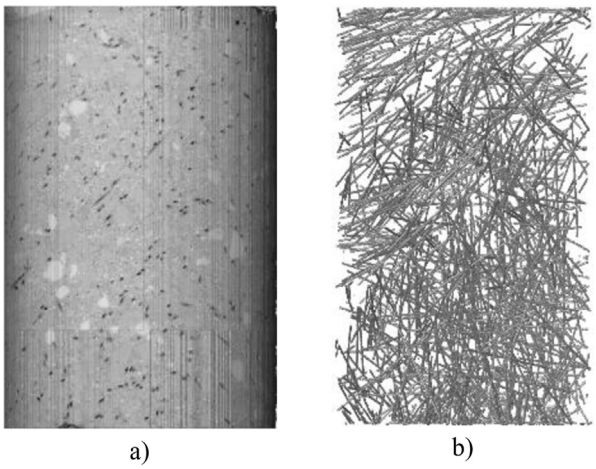

FIGURE 1
XRCT-scan of a 20 mm core drilled from a M2.0 sample **(A)** raw section through the sample **(B)** post-processed image with isolated PVA fibers.

a value of 80 µm pose only a limited threat to the structure since such narrow cracks do not allow enough water and harmful ions to enter the crack (Wang et al., 1997; Şahmaran and Li, 2010). The range of 100–120 µm was chosen in order to evaluate whether the material is able to also heal cracks that pose a risk to the durability of the structure. A 3PBT with a support span of 230 mm was used to accurately create a crack width in this range. The crack opening at the bottom of the samples was measured with a linear variable differential transformer (LVDT). After 28 days from casting, specimens were subjected to loading in a displacement-controlled regime with a speed of 0.1 mm/min. The target was to create one single crack with a crack opening within a range of 100–120 µm. Due to the viscoelastic re-deformation of the crack after unloading caused by the PVA fibers, it was necessary to load the samples to a crack opening of 250 µm. After the viscoelastic re-deformation subsided, a remaining crack opening of 100–120 µm was achieved. All cracks were additionally identified and recorded using the high-resolution camera described in Section 2.4.

2.5.2 Self-healing methodology

After pre-cracking, all samples of the series HEAL14, RECRK14, HEAL28, and RECRK28 were immersed in a tank filled with tap water at room temperature to simulate self-healing for 14 and 28 days respectively. The chloride content of the tap water used for this study is very low at 11.5 mg per liter (Harzwasserwerke GmbH, 2022) and no measurable impact of chloride contamination was found during preliminary test batches with tap water. After the healing period, samples were taken out of the water tank and dried in the oven for 24 h at 60°C before continuing with the chloride penetration or stiffness recovery tests.

2.5.3 Chloride penetration test

In this study, chloride permeability in the cracked state was analyzed as a way to measure the durability properties of the material and its ability to recover these durability properties through self-healing. The chloride permeability was evaluated through pigmentation with silver nitrate ($AgNO_3$), a fairly simple yet reliable technique to visualize chloride penetration (Otsuki et al., 1993; Baroghel-Bouny et al., 2007). The experimental procedure largely follows the methodology

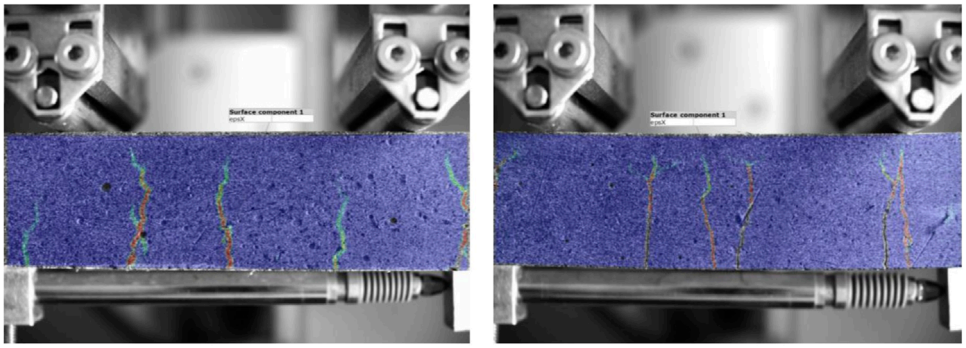

FIGURE 2
Cracking pattern (4PBT) visualized by DIC after 56 days for specimens **(A)** M1.5- ULT56-2 and **(B)** M2.0-ULT56-2.

proposed by Doostkami et al. (Doostkami et al., 2021) with a few modifications made to better fit the goals of this work. This procedure was done for cracked samples (CRK) and cracked samples healed for 14 (HEAL14) and 28 days (HEAL28) of both mixes.

First, samples are pre-cracked to a remaining crack opening in the range of 100–120 µm, as previously explained in Section 2.5.1. After, the beams were turned around and PVC-tubes were attached with a fast-setting, impermeable glue. The tubes were placed directly on the crack in the center of the beam. The tubes were then filled with a 3.5% NaCl solution. Exposure was maintained for 72 h. Figure 3 illustrates the setup and its sequential steps. After exposure, the tubes were emptied and removed from the samples. The samples were put in the oven to dry for 24 h at 60°C. After drying, the samples were sawed with a circular concrete saw along the center of the beam, perpendicular to the crack. Special care was taken during the sawing process to prevent contamination of the section and to avoid washing out superficial chlorides. To this end, the saw rotation was selected to cut from the tip of the crack towards the surface of the exposed side.

After sawing, the samples were again left to dry in the oven for 24 h at 60°C. To evaluate the chloride penetration, a silver nitrate solution ($AgNO_3$) was prepared at a concentration of 0.1 mol/L. After spraying the surfaces of the samples with the silver nitrate solution, they were once again put in the oven under the aforementioned conditions for 24 h to improve the pattern display. The silver nitrate reacts with chlorides forming white crystals, while dark areas highlight the absence of chlorides. Images of the resulting patterns after drying were taken with a high-resolution digital camera. Each image was then binarized to highlight the penetration area. From these images the chloride penetration through the matrix (P_0), penetration depth (P_d), and penetration width (P_w) were obtained, which served as a measure to compare the different samples.

These measurements can then be used to calculate a durability recovery index. Equation 1 shows the formula that quantifies the re-establishment of the uncracked state with regard to chloride penetration. A reduction of the penetration depth P_d to P_0 is considered a full recovery of the durability, representing the uncracked state.

$$\text{Durability recovery index } [\%] = \frac{(P_d - P_0)_{\text{unhealed}} - (P_d - P_0)_{\text{healed}}}{(P_d - P_0)_{\text{unhealed}}} \text{ x } 100 \quad (1)$$

2.5.4 Stiffness recovery analysis

Even though a crack may appear fully healed and exhibit a significantly increased resistance to the penetration of potentially harmful ions, the strength of these newly formed reaction products should be questioned. One way to quantify the strength of the sealed cracks is through a stiffness recovery analysis that has been used for ECCs (Ma et al., 2019) as well as other fiber-reinforced composites (Monte and Ferrara, 2021). To that end, a separate set of specimens (RECRK14 and RECRK28) were tested in terms of strength of the healed cracks after different healing periods. These beams were tested in the same 3PBT-setup used for the pre-cracking process, guaranteeing that the peak stress occurs in the healed crack. All test variables were kept the same with the exception of the loading speed, which was reduced to 0.025 mm/min up to a displacement of 0.1 mm in order capture the precise point at which the healed crack reopens. When loaded, these healed beams exhibit a short linear elastic response until the load-carrying capacity of the healed crack is exceeded and fracture occurs. After this point the stress-strain curve becomes flatter as the fibers are activated. With the help of time-stamped DIC it is possible to clearly identify the point on the stress-displacement curve at which the healed crack opens again. It is then possible to calculate the secant stiffness of the healed crack and compare it to the initial stiffness of the uncracked specimen.

3 Results and discussions

3.1 Pre-cracking

All samples that were later exposed to chloride penetration or analyzed in terms of their stiffness recovery were subjected to pre-cracking in a 3PBT. Figure 4 shows the remaining crack widths

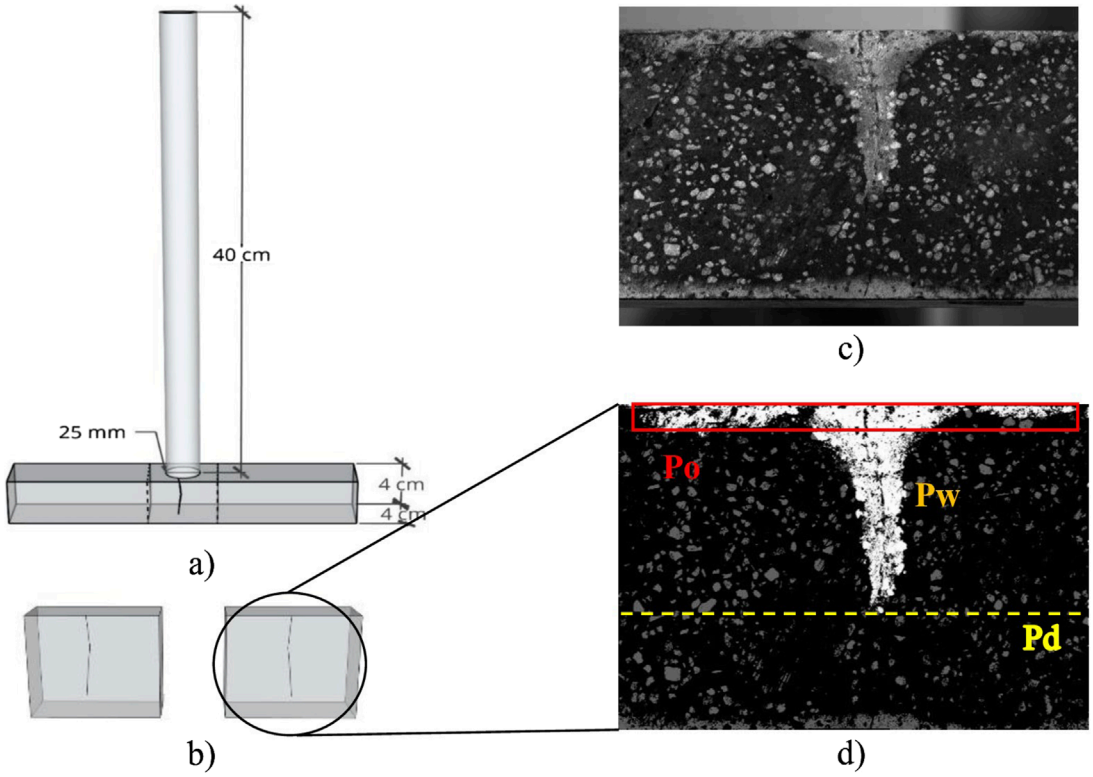

FIGURE 3
Setup of the chloride permeability test as **(A)** beam with the PVC tube attached, **(B)** sections obtained after the cut, **(C)** example of a high-resolution image obtained after spraying with AgNO3 and drying, **(D)** binarized image.

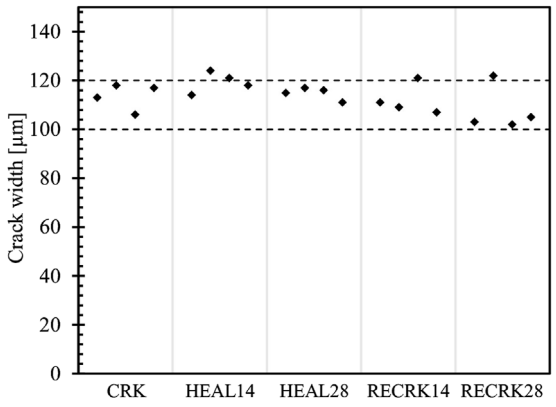

FIGURE 4
Recorded remaining crack widths after pre-cracking for all series.

recorded after unloading grouped by series. The targeted crack opening width was 100–120 µm.

With the exception of four samples where the cracks slightly exceed the upper limit, all samples fell within the targeted range. It is important to note that the recorded crack widths are those recorded several minutes after unloading the samples. This allows for the viscoelastic re-deformation after unloading to subside so that the recorded crack widths represent the widths that are exposed to chlorides or the healing process in the subsequent steps.

3.2 Chloride penetration

A series of chloride penetration tests were performed in order to evaluate the durability properties and to quantify to which extent it is able to reestablish its resistance to chloride penetration through self-healing.

Figures 5–7 present the binarized images obtained after submitting unhealed samples (Figure 5), samples healed for 14 days (Figure 6), and samples healed for 28 days (Figure 7) to a chloride solution for 72 h. Areas where chlorides penetrated the samples are shown in white through a chemical reaction with silver nitrate. The authors chose to represent the penetration through the matrix (P_0) using a rectangular box and to indicate the penetration through the crack, defined as the penetration depth (P_d), using a dashed line. This was done in order to differentiate the two modes of penetration. Table 5 lists all the measured values for P_d and P_0 which served as a basis for the calculation the durability recovery indices.

In Figure 5, results for the unhealed samples exposed right after pre-cracking are shown. Regarding P_0, the penetration front was quite clearly discernable and no significant difference between the two mixes could be observed. The matrix penetration depth P_0 measures around 2–3 mm in all samples. The ingress of chlorides through the matrix was limited to a few millimeters due to the

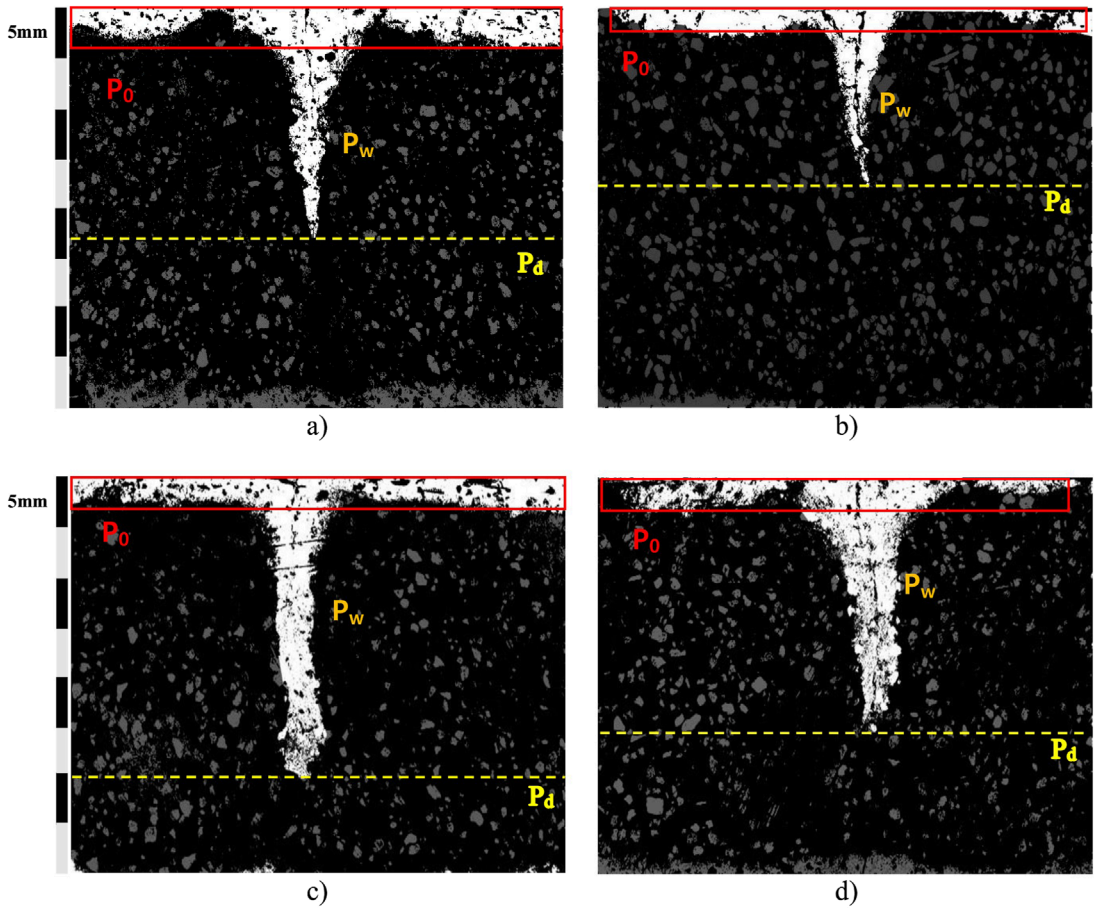

FIGURE 5
Binarized images of pre-cracked samples (CRK) for **(A, B)** M1.5 **(C, D)** M2.0.

fine composition of the material and the consequently high quality with respect to porosity (Saha, 2018; Chindaprasirt et al., 2007). For the chloride penetration through the cracks, here described as the penetration depth P_d, the penetration reaches deep into the crack. During the experiment it was noticeable that after a few minutes water droplets could be seen leaking out of the sides of the crack. A penetration depth P_d ranging from 15 mm to 27 mm was measured, as shown in Table 5. A significant lateral penetration of chlorides from the crack walls into the matrix appears alongside the penetration of the cracks. This penetration width P_w is conically shaped indicating that the chloride solution takes longer to reach the crack tip and therefore has less time to penetrate laterally. Closer to the exposure surface, values for P_w are larger and measurements are comparable to P_0. It is also evident that there is a larger lateral penetration through the crack walls P_w in M2.0 samples, which can be attributed to the less dense matrix after only 28 days of curing due to the higher fly ash content.

Figure 6 shows results for samples that were pre-cracked and healed for 14 days before exposure. First, penetration through the uncracked matrix P_0 is reduced when compared to the unhealed samples. While before, the entire surface was susceptible to chloride penetration in the unhealed samples, it is now restricted to localized penetration patches that are also shallower than before. This development is separated from the healing in the crack and is caused by the continued pozzolanic reaction in the specimens during water immersion. The high content of fly ash in both mixes facilitates the steady densification of the matrix (Lorenzo et al., 2002). As reaction products fill pore space, the material's permeability is reduced. Second, the penetration depth P_d approaches P_0 in many of the samples, indicating that the crack no longer represents a local defect with greater penetration depth than the uncracked bulk material. This is evident in all samples with the exception of the one shown in Figure 6A where P_d is still larger than P_0, yet notably reduced compared to the unhealed samples. Because of the lack of a clear crack penetration in most samples, it was no longer possible to define P_w. The durability recovery index calculated for samples healed for 14 days ranged from 81.1% to 99.6%, proving that crack sealing is already very effective after 14 days of healing.

The results obtained for specimens healed for 28 days after pre-cracking are presented in Figure 7. In line with the previously observed trend, the penetration of chlorides is further reduced. With the exception of the sample shown in Figure 7D, the penetration depth P_d has been reduced to P_0, leading to durability recovery indices ranging from 84.1% to 100%.

Autogenous self-healing is largely governed by continued reaction of unhydrated cement, the recrystallization of portlandite

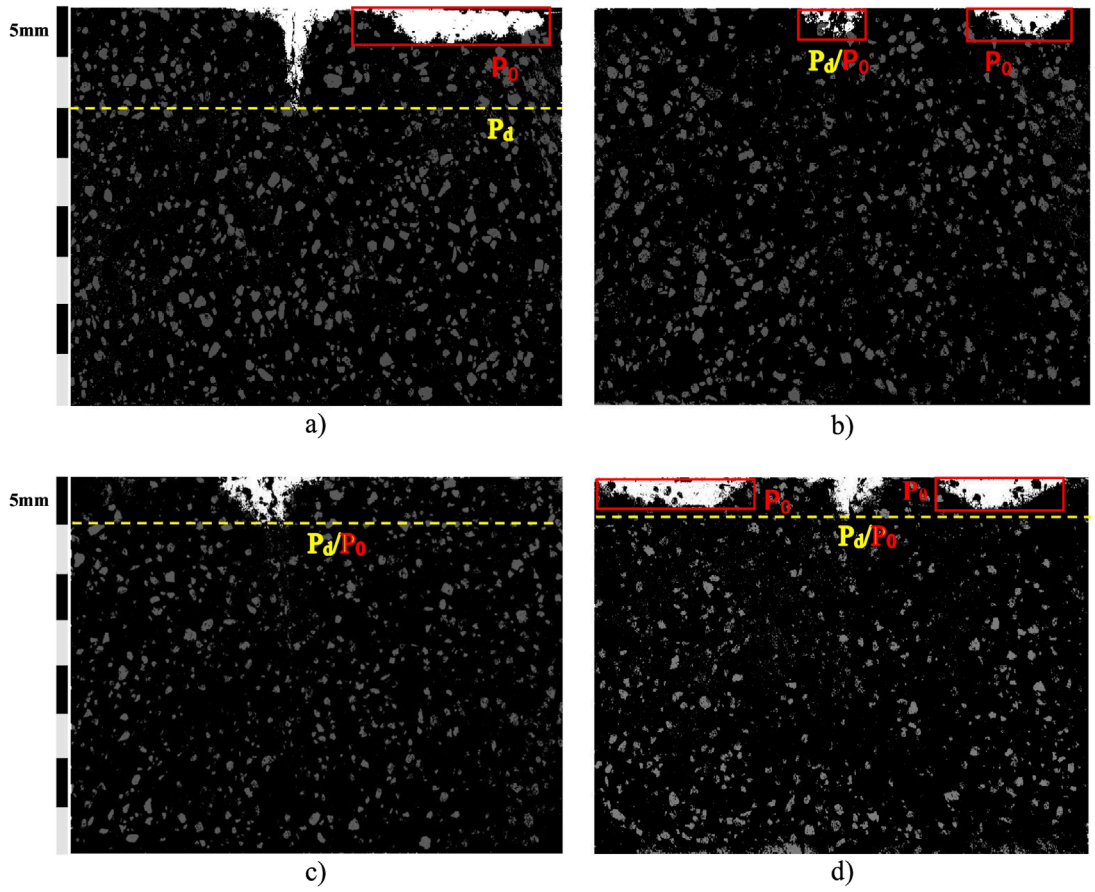

FIGURE 6
Binarized images of samples after 14 days of healing (HEAL14) for **(A, B)** M1.5 **(C, D)** M2.0.

leaching from the bulk paste, and the formation of calcite (Huang et al., 2016). While the addition of fly ash has been reported to improve self-healing efficiency (Huang et al., 2016), higher amounts of fly ash can have a negative effect on self-healing due to the depletion of $Ca(OH)_2$ leading to a lower concentration of Ca^{2+} ions in the crack (Rajczakowska et al., 2023). Comparing the two mix designs with different levels of fly ash, mix M2.0 with higher fly ash content appears to perform better in terms of crack sealing after 14 days with a durability recovery index of 99.6% compared to 81.1% for M1.5. After 28 days, however, M1.5 performs better with 100% durability recovery vs. 84.1% for M2.0. Therefore, while both mixes perform extremely well with durability recovery indices between 80% and 100% in all cases, no clear statement can be made as to which composite performs better. The scatter in the test data can likely be attributed to factors such as tortuosity or locally varying crack widths affecting individual test results.

In summary it can be stated that self-healing effectively reduces the penetration of chlorides through cracks exceeding 100 µm. Even if not all cracks were fully sealed, it is a very effective mechanism to re-establish the protective properties of a concrete cover with the durability recovery index exceeding 80% in every sample. The fact that the largest part of the reaction takes place during the first 14 days is additionally encouraging, as it ensures vulnerabilities in the material caused by cracking only persist for a short period of time. Using a durability recovery index can be a valuable measure to quantify this effect on the durability properties of fiber-reinforced composites after cracking.

3.3 Stiffness recovery

Figure 8 shows the stress–crack mouth opening displacement (CMOD) curves of samples M1.5-RECRK14–1 and M2.0-RECRK14-1. As elaborated in Section 3.1, the samples were first loaded to a CMOD of 250 µm during the pre-cracking process and then unloaded. For both samples, the targeted remaining CMOD of 100–120 µm was reached after the viscoelastic crack closure subsided. After 14 days of healing the samples were loaded again. The loading curve after healing is offset by the remaining CMOD after pre-cracking in Figure 8 and shown as a dashed line.

It can be seen that the stress-CMOD curve continues on its initial path and in both cases exhibits strain hardening, exceeding the first-cracking stress. Shown in green are the initial elastic tangents of the uncracked samples calculated from the linear elastic part of the curve before the first crack appears. The green line is shifted in the plot to the point at which the specimens are re-loaded after healing for better comparison with the tangent after healing, which is shown in red. By comparing the two plots it appears that the

10.3389/fmats.2024.1443216

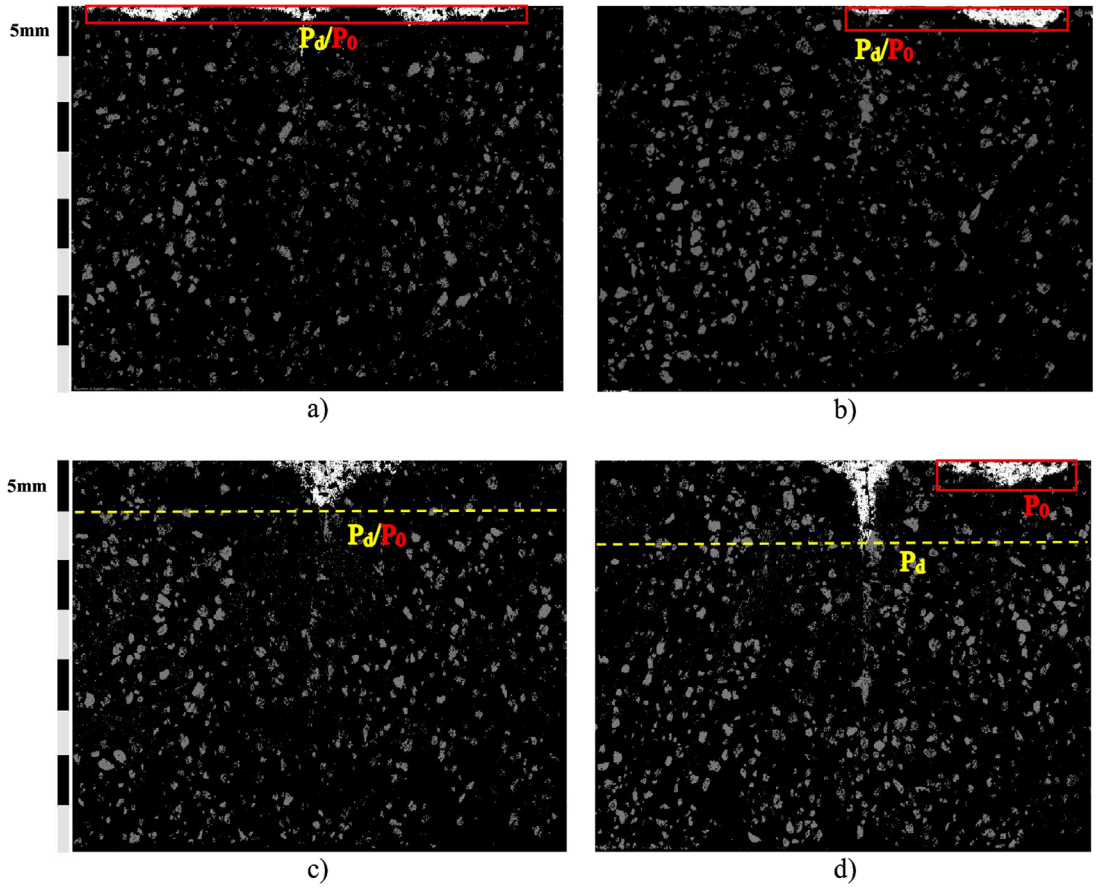

FIGURE 7
Binarized images of samples after 28 days of healing (HEAL28) for **(A, B)** M1.5 **(C, D)** M2.0.

TABLE 5 Penetration values obtained for each sample of all series and the calculated durability recovery index.

Series	P_d [mm]	P_0 [mm]	P_d - P_0 [mm]	Average (P_d - P_0) [mm]	Durability recovery index [%]
CRK-M1.5	23.0	4.0	19.0	17.3	N/A
	17.5	2.0	15.5		
CRK-M2.0	30.0	3.0	27.0	24.5	N/A
	25.0	3.0	22.0		
HEAL14-M1.5	10.0	3.5	6.5	3.3	81.1
	3.5	3.5	0		
HEAL14-M2.0	5.0	5.0	0	0.1	99.6
	5.0	4.8	0.2		
HEAL28-M1.5	1.5	1.5	0	0	100
	2.0	2.0	0		
HEAL28-M2.0	5.0	5.0	0	2.8	84.1
	8.5	3.0	5.5		

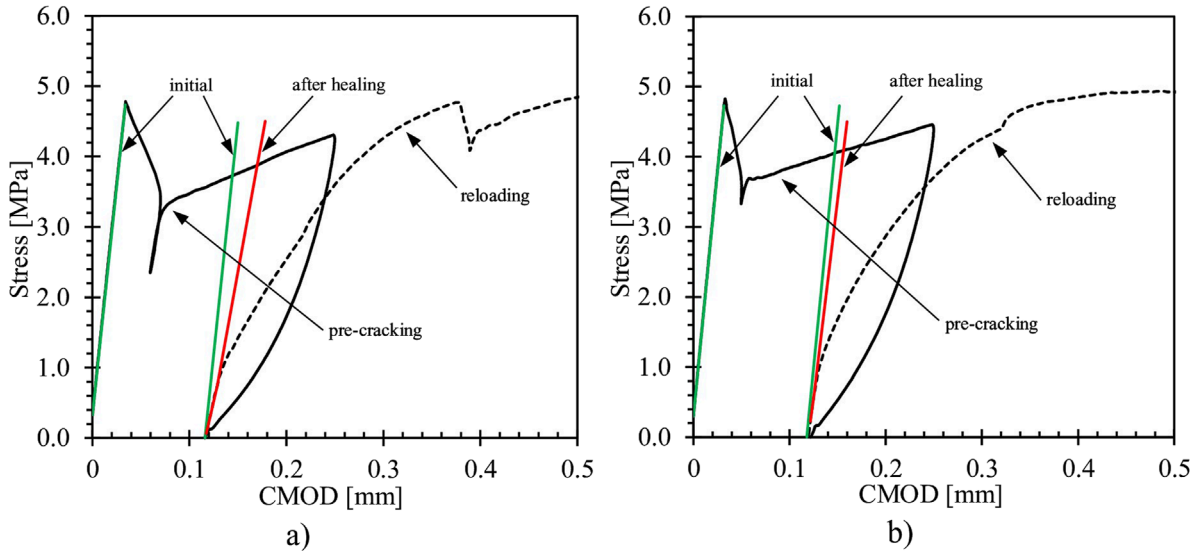

FIGURE 8
Stress-CMOD graphs of reloaded samples with the initial elastic modulus (green) compared to the elastic modulus after 14 days of healing (red) for **(A)** M2.0-RECRK14-1 **(B)** M1.5-RECRK14-1.

stiffness recovery, i.e., the elastic modulus after healing compared to the initial elastic modulus, is greater for the M1.5 mix compared to the M2.0 mix.

To verify this observation, all measurements of the RECRK-series for both 14 and 28 days were plotted in Figure 9. The figure compares the stiffness recovery expressed in percent compared to the initial stiffness of the respective samples measured during the pre-cracking process. It becomes evident that throughout the series, mix M1.5 performs better in terms of strength of the healed cracks with a stiffness recovery of about 60%. For both 14 and 28 days, the observed stiffness recovery is greater than for the M2.0 mix, which only reaches a stiffness recovery of about 40%–50% for 14 and 28 days respectively. The apparently greater loss of stiffness of the M1.5 series after 28 days compared to 14 days does not appear plausible and is contrary to what is observed for the M2.0 series. It is, however, most likely influenced by the great variance within the individual datapoints of the M1.5 series. A larger number of samples would be necessary to reduce the variance and make a more accurate statement about the influence of a longer healing period. Notwithstanding, it can be observed that healing takes place mainly within the first 14 days with results not improving significantly after 28 days. This observation agrees with the results of the chloride penetration tests.

Generally, it is important to point out that while the stiffness recovery analysis showed the formation of stronger healing products in composites with higher cement content, the stiffness of the uncracked material is never fully recovered. It appears that while both mixes succeed at physically sealing the cracks there is a significant difference in the strength of the newly formed reaction products. This, in turn, implies that enhancing sustainability by reducing cement content does not measurably affect the material's durability properties. It does, however, reduce the strength of the healed cracks.

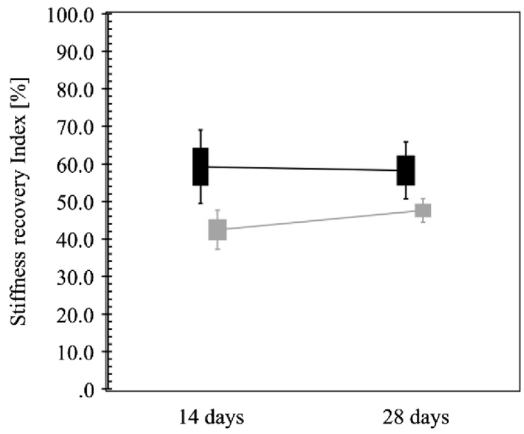

FIGURE 9
Elastic moduli of series M1.5 (black) and M2.0 (gray) healed for 14 and 28 days relative to the initial elastic modulus of the respective samples.

4 Conclusion and further research

In this study, two different mix designs of PVA fiber-reinforced cementitious composites were investigated using comparative chloride penetration tests. Two different mix designs with a varying cement to fly ash ratio of 1:1.5 and 1:2.0 were studied under the influence of different healing periods up to 28 days. Chloride penetration resistance as well as the stiffness recovery associated with the healed cracks were analyzed. The main conclusions are summarized as follows:

- A durability recovery index was proposed to quantify the material's ability to re-establish its durability properties

after cracking through self-healing. The approach uses an experimental setup that is easy to replicate and gives reliable, quantitative results indicating the chloride penetration resistance of the material.

- Samples of both mixes were exposed to a chloride solution for 72 h after inducing cracks in a range of 100–120 µm. Results showed that crack sealing is already very effective after 14 days of healing. Chloride penetration was significantly reduced, with durability recovery index values ranging from 81.1% to 99.6%. Penetration through the matrix is also reduced when compared to the unhealed samples. After 28 days of self-healing, the penetration of chlorides is further reduced to durability recovery index values between 84.1% and 100%. The benefit of longer self-healing periods appears to be limited, indicating that a large part of the reaction in the crack concluded after 14 days. Further tests of samples exposed to fewer days of healing could yield valuable results regarding the early stages of self-healing.
- Stiffness recovery was analyzed after 14 and 28 days of self-healing. 40%–60% of the initial stiffness could be recovered by self-healing and higher stiffness recovery was found to correlate with higher cement content for both healing periods. The results can provide valuable insight for future research investigating cyclic loading during the healing process. Repeated loading of the specimens can significantly impact the material's ability to self-heal by re-fracturing freshly formed hydration products. It is therefore of great relevance to know the range in which the healed crack behaves elastically and no damage occurs in the healed crack. One possible approach could be to limit loads to below what the cracks can sustain without fracture.

Self-healing in cementitious composites effectively and quickly reduces the diffusivity of chlorides while stiffness recovery is limited. This makes them a suitable material in aggressive environments where durability limits a structure's lifespan. Further investigations with larger sample numbers are necessary to more precisely quantify the effects of the binder composition on the reduction of penetration to chlorides.

Data availability statement

The raw data supporting the conclusions of this article will be made available by the authors, without undue reservation.

Author contributions

UB: Formal Analysis, Investigation, Methodology, Writing–original draft. EC: Writing–review and editing. RJ: Conceptualization, Supervision, Writing–review and editing. TT: Conceptualization, Formal Analysis, Methodology, Visualization, Writing–review and editing.

Funding

The author(s) declare that financial support was received for the research, authorship, and/or publication of this article. The support of the German Research Foundation (DFG) in the framework of the Research Training Group 2075/2 "Modeling the constitutive evolution of building materials and structures with respect to aging" is gratefully acknowledged. We acknowledge the support by the Open Access Publication Funds of Technische Universität Braunschweig.

Conflict of interest

The authors declare that the research was conducted in the absence of any commercial or financial relationships that could be construed as a potential conflict of interest.

Publisher's note

References

Alexander, M., and Beushausen, H. (2019). Durability, service life prediction, and modelling for reinforced concrete structures–review and critique. *Cem. Concr. Res.* 122, 17–29. doi:10.1016/j.cemconres.2019.04.018

Baroghel-Bouny, V., Belin, P., Maultzsch, M., and Henry, D. (2007). AgNO 3 spray tests: advantages, weaknesses, and various applications to quantify chloride ingress into concrete. Part 2: non-steady-state migration tests and chloride diffusion coefficients. *Mater. Struct.* 40, 783–799. doi:10.1617/s11527-007-9236-y

Bijen, J. (2003). *Durability of engineering structures: design, repair and maintenance*. Elsevier.

Cai, J., Pan, J., Lin, Y., Han, J., Ding, B., and Ukrainczyk, N. (2023). Effect of temperature on the low-velocity impact behaviors of engineered cementitious composite. *J. Mater. Civ. Eng.* 35 (7), 04023167. doi:10.1061/jmcee7.mteng-15023

Casini, M. (2022). *Construction 4.0: advanced technology, tools and materials for the digital transformation of the construction industry*. Cambridge, United Kingdom: Woodhead Publishing, 337–404.

Chen, G., Tang, W., Chen, S., Wang, S., and Cui, H. (2022). Prediction of self-healing of engineered cementitious composite using machine learning approaches. *Appl. Sci.* 12 (7), 3605. doi:10.3390/app12073605

Chindaprasirt, P., Chotithanorm, C., Cao, H. T., and Sirivivatnanon, V. (2007). Influence of fly ash fineness on the chloride penetration of concrete. *Constr. Build. Mater.* 21 (2), 356–361. doi:10.1016/j.conbuildmat.2005.08.010

Doostkami, H., Roig-Flores, M., and Serna, P. (2021). Self-healing efficiency of ultra high-performance fiber-reinforced concrete through permeability to chlorides. *Constr. Build. Mater.* 310, 125168. doi:10.1016/j.conbuildmat.2021.125168

Felekoglu, B., Tosun-Felekoglu, K., Ranade, R., Zhang, Q., and Li, V. C. (2014). Influence of matrix flowability, fiber mixing procedure, and curing conditions on the mechanical performance of HTPP-ECC. *Compos. Part B Eng.* 60, 359–370. doi:10.1016/j.compositesb.2013.12.076

França, M. S. D. (2018). *Rheological behavior of engineered cementitions composites reinforced with PVA fibers*. Sao Paulo, Brazil: Doctoral dissertation, Universidade de São Paulo.

Harzwasserwerke GmbH (2022). Trinkwasseranalyse– Mittel-, Minimum-Maximumwerte aus den Monatsanalysen 2022 für HB-Lindenberg/MW Ecker + Grane. Available at: https://www.harzwasserwerke.de/wp-content/uploads/2023/11/hb_lin.pdf.Retrieved 08 February 2023

Huang, H., Ye, G., Qian, C., and Schlangen, E. (2016). Self-healing in cementitious materials: materials, methods and service conditions. *Mater. and Des.* 92, 499–511. doi:10.1016/j.matdes.2015.12.091

Jiangtao, Y., Fangming, J., Qiong, X., Qi, Y., and Mi, L. (2021). Mechanical and self-healing performances of crumb rubber modified high-strength engineered cementitious composites. *Front. Mater.* 8, 811110. doi:10.3389/fmats.2021.811110

Kang, S. T., and Kim, J. K. (2011). The relation between fiber orientation and tensile behavior in an ultra high performance fiber reinforced cementitious composites (UHPFRCC). *Cem. Concr. Res.* 41 (10), 1001–1014. doi:10.1016/j.cemconres.2011.05.009

Krentowski, J. R. (2021). Assessment of destructive impact of different factors on concrete structures durability. *Materials* 15 (1), 225. doi:10.3390/ma15010225

Lepech, M. D., and Li, V. C. (2009). Water permeability of engineered cementitious composites. *Cem. Concr. Compos.* 31 (10), 744–753. doi:10.1016/j.cemconcomp.2009.07.002

Li, V. C. (1992). Postcrack scaling relations for fiber reinforced cementitious composites. *J. Mater. Civ. Eng.* 4 (1), 41–57. doi:10.1061/(asce)0899-1561(1992)4:1(41)

Li, V. C. (1993). From micromechanics to structural engineering the design of cementitious composites for civil engineering applications. *Dob. Gakkai Ronbunshu* 1993 (471), 1–12. doi:10.2208/jscej.1993.471_1

Li, V. C. (1998). Engineered cementitious composites (ECC)-tailored composites through micromechanical modeling.

Li, V. C. (2019). *Engineered cementitious composites (ECC): bendable concrete for sustainable and resilient infrastructure*. Springer.

Li, V. C., Wang, S., and Wu, C. (2001). Tensile strain-hardening behavior of polyvinyl alcohol engineered cementitious composite (PVA-ECC). *Mater. J.* 98 (6), 483–492.

Lorenzo, M. P., Goñi, S., and Guerrero, A. (2002). Activation of pozzolanic reaction of hydrated portland cement fly ash pastes in sulfate solution. *J. Am. Ceram. Soc.* 85 (12), 3071–3075. doi:10.1111/j.1151-2916.2002.tb00581.x

Ma, H., Herbert, E., Ohno, M., and Li, V. C. (2019). Scale-linking model of self-healing and stiffness recovery in Engineered Cementitious Composites (ECC). *Cem. Concr. Compos.* 95, 1–9. doi:10.1016/j.cemconcomp.2018.10.006

Mehta, P. K. (1991). "Durability of concrete—fifty years of progress?," in SP-126: Durability of Concrete: Second International Conference, Montreal, Canada.

Monte, F. L., and Ferrara, L. (2021). Self-healing characterization of UHPFRCC with crystalline admixture: experimental assessment via multi-test/multi-parameter approach. *Constr. Build. Mater.* 283, 122579. doi:10.1016/j.conbuildmat.2021.122579

Neville, A. (2001). Consideration of durability of concrete structures: past, present, and future. *Mater. Struct.* 34, 114–118. doi:10.1007/bf02481560

Otsuki, N., Nagataki, S., and Nakashita, K. (1993). Evaluation of the AgNO3 solution spray method for measurement of chloride penetration into hardened cementitious matrix materials. *Constr. Build. Mater.* 7 (4), 195–201. doi:10.1016/0950-0618(93)90002-t

Öztürk, O., Yıldırım, G., Keskin, Ü. S., Siad, H., and Şahmaran, M. (2020). Nano-tailored multi-functional cementitious composites. *Compos. Part B Eng.* 182, 107670. doi:10.1016/j.compositesb.2019.107670

Passuello, A., Moriconi, G., and Shah, S. P. (2009). Cracking behavior of concrete with shrinkage reducing admixtures and PVA fibers. *Cem. Concr. Compos.* 31 (10), 699–704. doi:10.1016/j.cemconcomp.2009.08.004

Plagué, T., Desmettre, C., and Charron, J. P. (2017). Influence of fiber type and fiber orientation on cracking and permeability of reinforced concrete under tensile loading. *Cem. Concr. Res.* 94, 59–70. doi:10.1016/j.cemconres.2017.01.004

Polder, R. B., Peelen, W. H. A., and Courage, W. M. G. (2012). NonNon-traditional assessment and maintenance methods for aging concrete structures – technical and non-technical issuestraditional assessment and maintenance methods for aging concrete structures–technical and non-technical issues. *Mater. Corros.* 63 (12), 1147–1153. doi:10.1002/maco.201206725

Rajczakowska, M., Tole, I., Hedlund, H., Habermehl-Cwirzen, K., and Cwirzen, A. (2023). Autogenous self-healing of low embodied energy cementitious materials: effect of multi-component binder and crack geometry. *Constr. Build. Mater.* 376, 130994. doi:10.1016/j.conbuildmat.2023.130994

Ruan, S., Qiu, J., Yang, E. H., and Unluer, C. (2021). Influence of crack width on the stiffness recovery and self-healing of reactive magnesia-based binders under CO2-H2O conditioning. *Constr. Build. Mater.* 269, 121360. doi:10.1016/j.conbuildmat.2020.121360

Saha, A. K. (2018). Effect of class F fly ash on the durability properties of concrete. *Sustain. Environ. Res.* 28 (1), 25–31. doi:10.1016/j.serj.2017.09.001

Şahmaran, M., and Li, V. C. (2010). Engineered cementitious composites: can composites be accepted as crack-free concrete? *Transp. Res. Rec.* 2164 (1), 1–8. doi:10.3141/2164-01

Sarmiento, E. V., Geiker, M. R., and Kanstad, T. (2016). Influence of fibre distribution and orientation on the flexural behaviour of beams cast from flowable hybrid polymer–steel FRC. *Constr. Build. Mater.* 109, 166–176. doi:10.1016/j.conbuildmat.2016.02.005

Shobana, K., Aarthi, R., Madhan, P., and Aparna, L. N. (2021). Self-healing concrete mix-design based on engineered cementations composites principles. *Int. J. Aquatic Sci.* 12 (3), 3140–3149.

Tawfek, A. M., Ge, Z., Yuan, H., Zhang, N., Zhang, H., Ling, Y., et al. (2023). Influence of fiber orientation on the mechanical responses of engineering cementitious composite (ECC) under various loading conditions. *J. Build. Eng.* 63, 105518. doi:10.1016/j.jobe.2022.105518

Wang, K., Jansen, D. C., Shah, S. P., and Karr, A. F. (1997). Permeability study of cracked concrete. *Cem. Concr. Res.* 27 (3), 381–393. doi:10.1016/s0008-8846(97)00031-8

Zeng, W., Ding, Y., Zhang, Y., and Dehn, F. (2020). Effect of steel fiber on the crack permeability evolution and crack surface topography of concrete subjected to freeze-thaw damage. *Cem. Concr. Res.* 138, 106230. doi:10.1016/j.cemconres.2020.106230

Zhu, M., Chen, B., Wu, M., and Han, J. (2022). Effects of different mixing ratio parameters on mechanical properties of cost-effective green engineered cementitious composites (ECC). *Constr. Build. Mater.* 328, 127093. doi:10.1016/j.conbuildmat.2022.127093